Meccanica
https://doi.org/10.1007/s11012-024-01853-8

RESEARCH

Rarefaction pulses on tensegrity lattices are just sech^2 -solitary (dark) waves

Julia de Castro Motta · Fernando Fraternali · Giuseppe Saccomandi

Received: 27 March 2024 / Accepted: 6 July 2024

Abstract This study investigates the propagation of rarefaction solitary waves in one-dimensional, tensegrity-like mass-spring lattices that are subject to an initial state of pre-compression. The analyzed systems exhibit a cubic interaction potential between adjacent masses that accurately captures the constitutive response of tensegrity prisms with elastically softening behavior. Analytical results are presented for the propagation of rarefaction solitary waves that produce a reduction of the initial prestress exhibited by the system. It is known in the literature that the use of cubic interaction potentials in one-dimensional lattices enables the prediction of the propagation of solitary waves with sech^2 profile. Investigating the particular case of pre-compressed, softening-type tensegrity lattices, this study shows that such a noticeable result can be derived using both the classical and the improved Boussinesq equation. The given results reveal the presence of rarefaction solitary waves in a suitable range of wave speeds, and offer an explicit formula for the upper bound of the rarefaction wave speed that leaves the system in a compressed state. The outcomes of the present work pave the way to the development of analytic models for the design of radically new, metamaterial-type impact protection systems. Numerical simulations show the ability of the tensegrity-like model in predicting the propagation of rarefaction solitary waves in a physical model of a tensegrity mass-spring chain.

Keywords Tensegrity · Solitary waves · Rarefaction · Boussinesq equation

1 Introduction

Solitary waves are pulses that travel in localized regions of space while maintaining a permanent form [1–3]. In the field of solid mechanics, such waves have been proved to exist in different media, such as continuum isotropic and anisotropic materials [4, 5], mechanical metamaterials [6, 7], and granular chains [8, 9]. While systems with a stiffening-type response have been demonstrated to support compression solitary waves under impact loading [2, 8], systems with a softening-type response are able to convert initially compressive impact loading into solitary rarefaction waves [6, 8, 10]. It is worth noting that the use of solitary wave dynamics has been proposed to design innovative acoustic applications of tensegrity structures, including next generation actuators and sensors, impact mitigation systems and adjustable focus acoustic lenses [11]. The use of tensegrity modules as unit cells of mechanical metamaterials has indeed led

J. de Castro Motta · F. Fraternali
Department of Civil Engineering, University of Salerno, Via Giovanni Paolo II, 132, 84084 Fisciano, SA, Italy

G. Saccomandi (✉)
Department of Engineering, University of Perugia, Via G. Duranti, 06124 Perugia, Italy
e-mail: giuseppe.saccomandi@unipg.it

Published online: 19 July 2024

to the design of novel devices supporting localized solitary waves under impact loading [12–14], in addition to tunable bandgap systems [15–18].

The present work deals with an analytic study of the solitary wave dynamics of one-dimensional chains formed by lumped masses alternating with externally pre-compressed minimal regular tensegrity prisms [19] ('*T*3 units'). Due to the complex behavior of the force versus displacement response of such units [20], it is not easy to obtain analytic results for the wave propagation problem in tensegrity metamaterials. The use of a 'tensegrity-like' potential, able to suitably mimic the nature of the force-displacement exhibited by the real unit cell, has been shown to be a good option to analytically study the propagation of compression solitary waves. Such a study has been conducted with reference to lattices formed by tensegrity prisms [13] and truncated tensegrity octahedrons [14], which exhibit an elastically hardening response. However, the tensegrity-like approach has not yet been applied to tensegrity lattices that exhibit an elastically-softening behavior. This paper aims to fill such a gap by employing the well-known Fermi–Pasta–Ulam (FPU) cubic interaction potential [21], previously widely employed to analyze the propagation of solitary waves in lattice structures of different type (refer, e.g., to [22–24] and references therein). The FPU potential is shown to effectively capture the constitutive response of softening-type *T*3 prisms under compression loading. Its use leads to analytically prove, for the first time, that chains formed by such units support dark solitary waves with a sech^2 shape. This important result can be found using both the classical Boussinesq wave equation (for weakly non-linear systems) or an improved version of the same equation, derived by Rosenau [1].

The paper is organized as follows. Section 2 describes the mechanical response of the analyzed tensegrity units, while 3 illustrates the fitting of the FPU interaction potential to experimental and numerical data concerned with the compression loading of *T*3 prisms. An analytic study of the solitary pulses that are supported by mass-spring systems formed by these systems is presented in Sect. 4. Section 5 illustrates comparisons between the theoretical predictions of 4 and the numerical results presented in [6]. Concluding remarks and directions for future research are finally presented in 6.

2 Tensegrity prisms with softening response

Let us consider the *T*3 prisms shown in Fig. 1a, whose bases are connected to lumped masses formed by massive circular discs. We assume that the nodes of prisms are free to slide tangentially against the terminal discs, so as that the twisting motion of the prisms is not transferred to the lumped masses. Hereafter, we will use the symbols p_0, h_0, d, m, $\bar{b}$, d_b, $\bar{\ell}$, $\bar{s}_v$, d_s and $\bar{\vartheta}$ to denote the (internal) pre-strain of the base strings, the initial (undeformed) height of the unit cell (under zero external force), the thickness of the massive discs, the mass of the discs, the rest length of the bars on the natural configuration, the diameter of the bars, the rest length of the base strings on the natural configuration, the rest length of the cross strings on the natural configuration, the diameter of the strings

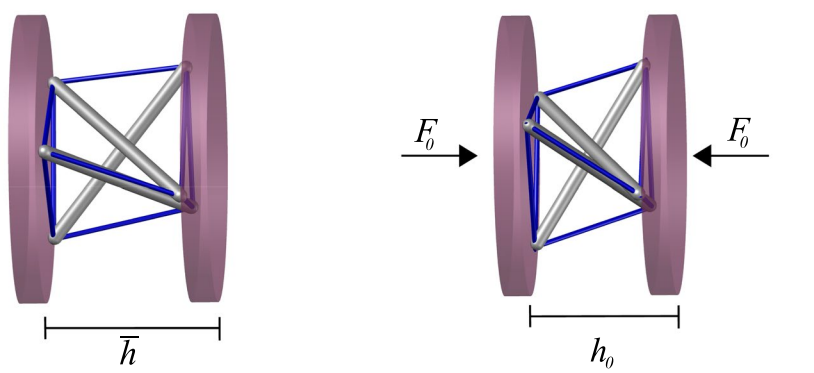

(a) Unloaded prism ($\hat{u} = 0$) (b) Initially pre-compressed prism ($\hat{u} = u_0$)

Fig. 1 Illustration of the unloaded (**a**) and pre-compressed (**b**) configurations of a *T*3 prism connected to lumped masses

and the initial twisting angle of the terminal bases, respectively.

Let now h denote the height of the unit cell in the current (deformed) configuration, which is given by $h = h_0 - \hat{u}$, where $\hat{u}$ is the relative axial displacement of the bases of the prism. The displacement $\hat{u}$ is produced by the action two compression forces $\hat{F}_{tens}$ applied to the centers of mass of such bases, and we can assume that the tensegrity unit is subject to an initial pre-compression force F_0, which prodduces the initial displacement $\hat{u} = u_0$, and the pre-compression strain $\epsilon_0 = u_0/h_0$ (Fig. 1b). We further introduce the quantities $u = \hat{u} - u_0$ and $F_{tens} = \hat{F}_{tens} - F_0$, and we let $h_{\epsilon_0} = h_0 - u_0$ denote the height of the prism under the action of the force F_0. All the forces and displacements will be assumed to be positive in compression in the remainder of the paper.

Previous experimental and mechanical studies have shown that $T3$ prisms exhibit an elastically-softening response for suitable values of the geometrical and prestress variable. In particular, the experimental study illustrated in [20] shows the achievement of such a regime in a macro-scale $T3$ prism equipped with the properties listed in Table 1, which we will refer to as unit #1. Such a system employs zinc plated steel bars with Young's modulus of 203.53 GPa and Spectra cables for the strings (Young modulus 5.48 MPa). The experimental axial force versus axial displacement response of this unit is illustrated in Fig. 2a, which exhibits a slope progressively decreasing with increasing values of $\hat{u}$, i.e., an elastically-softening behavior.

A numerical study on the response of a millimeter-scale $T3$ prism, which shows the proprieties listed in Table 2 (hereafter referred to as $T3$ units #2), has been presented in [6], observing the occurrence of a softening-type response also in this micro-scale system (see Fig. 2b). The bars of the unit #2 can be 3D-printed making use of electron beam melting and the Ti6Al4V titanium alloy (Young modulus 120 MPa), while the

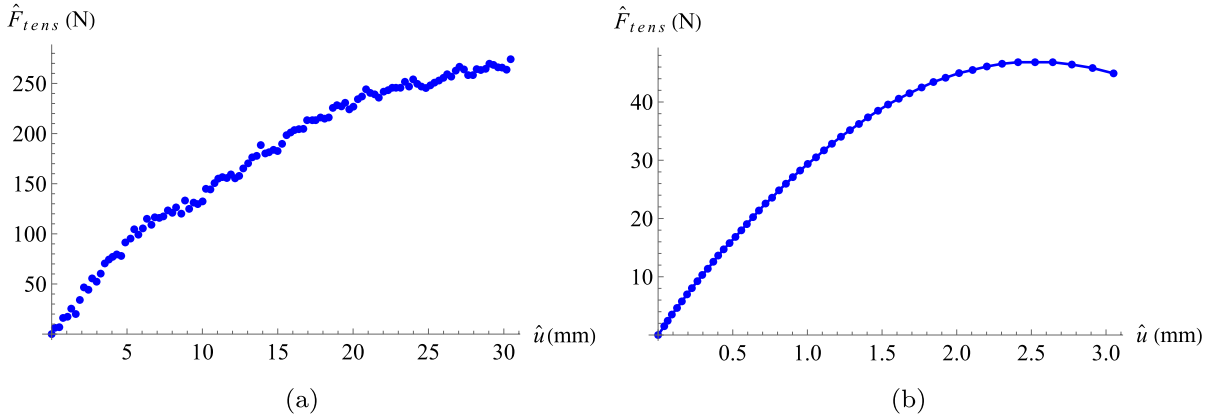

Fig. 2 Experimental force-displacement response of the $T3$ unit #1 under compression loading [20] (**a**) and numerical force-displacement response of the $T3$ unit # 2 [6] (**b**)

Table 1 Geometrical and mechanical properties of the $T3$ unit # 1 [20]

p_0 %	h_0 (mm)	$\bar{b}$ (mm)	d_b (mm)	$\bar{\ell}$ (mm)	$\bar{s}_v$ (mm)	d_s (mm)	$\bar{\vartheta}$ (deg)
7	74	174	6.83	132	80	0.76	150

Table 2 Geometrical and mechanical properties of the $T3$ unit #2 [6]

p_0 %	h_0 (mm)	$\bar{b}$ (mm)	d_b (mm)	$\bar{\ell}$ (mm)	$\bar{s}_v$ (mm)	d_s (mm)	d (mm)	m (g)	$\bar{\vartheta}$ (deg)
4	7.63	11.50	0.80	8.70	6.00	0.28	2.00	25	150

strings are again assumed to be made of Spectra cables, as in the case of unit # 1.

3 Cubic tensegrity-like interaction potential

The present section analyzes the use of the FPU cubic interaction potential defined by the following equation, with the aim of describing the response of the $T3$ units illustrated in the previous section

$$\hat{V}(\hat{u}) = \frac{1}{2}\hat{\alpha}_1\,\hat{u}^2 + \frac{1}{3}\hat{\alpha}_2\,\hat{u}^3, \tag{1}$$

where $\hat{\alpha}_1$ and $\hat{\alpha}_2$ are constitutive parameters. Such a classical potential has been often used for the development of weakly non-linear theories of lattice structures (see, e.g., [21–24] and references therein). Using the index notation for the derivatives with respect to $\hat{u}$, it is easy to obtain the force $\hat{F}$ versus displacement $\hat{u}$ law corresponding to the FPU cubic model in the form

$$\hat{F}(\hat{u}) = V_{\hat{u}} = \hat{\alpha}_1\,\hat{u} + \hat{\alpha}_2\,\hat{u}^2 \tag{2}$$

and for the stiffness coefficient the expression

$$\hat{k}(\hat{u}) = V_{\hat{u}\hat{u}} = \hat{\alpha}_1 + 2\,\hat{\alpha}_2\,\hat{u} \tag{3}$$

Equations (1)–(3) are employed in this work to develop a tensegrity-like model of the axial response of softening-type $T3$ tensegrity units from the natural (stress-free) state. The incremental response from the pre-compressed state will be instead described by the potential $V(u)$, the incremental force $F(u) = \hat{F}(u + u_0) - F_0$ and the incremental stiffness $k(u)$ defined as follows

$$V(u) = \frac{1}{2}\alpha_1\,u^2 + \frac{1}{3}\alpha_2\,u^3, \quad F(u) = \alpha_1\,u + \hat{\alpha}_2\,u^2, \quad k(u) = \alpha_1 + 2\,\alpha_2 u \tag{4}$$

where

$$\alpha_1 = \hat{\alpha}_1 + 2\,\hat{\alpha}_2\,\epsilon_0\,h_0, \qquad \alpha_2 = \hat{\alpha}_2 \tag{5}$$

Figure 3a, b, c graphically illustrate the V versus u, F versus u and k versus u laws, which are derived from Eq. (4) for given values of the constitutive parameters α_1 and α_2. It is easily observed that the response laws defined by the blue and green curves describe a system with elastically-stiffening behavior ($\alpha_1 > 0$, $\alpha_2 > 0$), while the red curves describe a system with elastically-softening response ($\alpha_1 > 0$, $\alpha_2 < 0$), which is of interest for the present research.

We now fit the cubic FPU model (4) to the responses of unit #1 (Fig. 2a) and unit #2 (Fig. 2b) described in the previous section. We obtain the best fit parameters $\hat{\alpha}_1 = 17.0371$ N/mm and $\hat{\alpha}_2 = -0.274523$ N/mm^2 with a coefficient of determination $R^2 = 0.998805$, using a dataset with 110 points for the response in Fig. 2a, and the *Mathematica*® function 'LinearModelFit'. Such a fitting procedure demonstrates that the cubic tensegrity-like model very well describes the observed experimental response of a softening-type $T3$ prism (see Fig. 4a, where the symbol $\hat{F}_{tens}$ marks the experimental data and the symbol $\hat{F}$ marks the tensegrity-like model).

Moving on to fit the tensegrity-like model to the response of unit #2, we employed a discretization with 51 points of the force-displacement curve illustrated in Fig. 2b and the *Mathematica*® function 'LinearModelFit' to obtain the best fit parameters $\hat{\alpha}_1 = 36.5921$ N/mm and $\hat{\alpha}_2 = -7.14109$ N/mm^2 ($R^2 = 0.999981$) (cf. Fig. 4b). The application of a pre-compression strain $\epsilon_0 = 0.15$ and the use of Eq. (5) leads us to obtain $\alpha_1 = 20.2462$ N/mm and $\alpha_2 = -7.14109$ N/mm^2 for the tensegrity-like model of the incremental response from the pre-compressed state, which is defined by Eq. (4).

4 The dark solitary wave

The Hamiltonian of a tensegrity mass-spring chain composed of n $T3$ prisms with a softening-type elastic response can be expressed as follows. We define x as the abscissa along the pre-compressed configuration of the chain, which we take as our reference. The symbols x_i and w_i represent the abscissa and the axial displacement of the i-th unit, respectively. By defining $u_i = w_{i-1} - w_i$, the Hamiltonian of the system is given by

$$H = \sum_{i=1}^{n-1}\left[\frac{1}{2}m\left(\frac{dw_i}{dt}\right)^2 + V\left(w_{i+1} - w_i\right)\right],$$

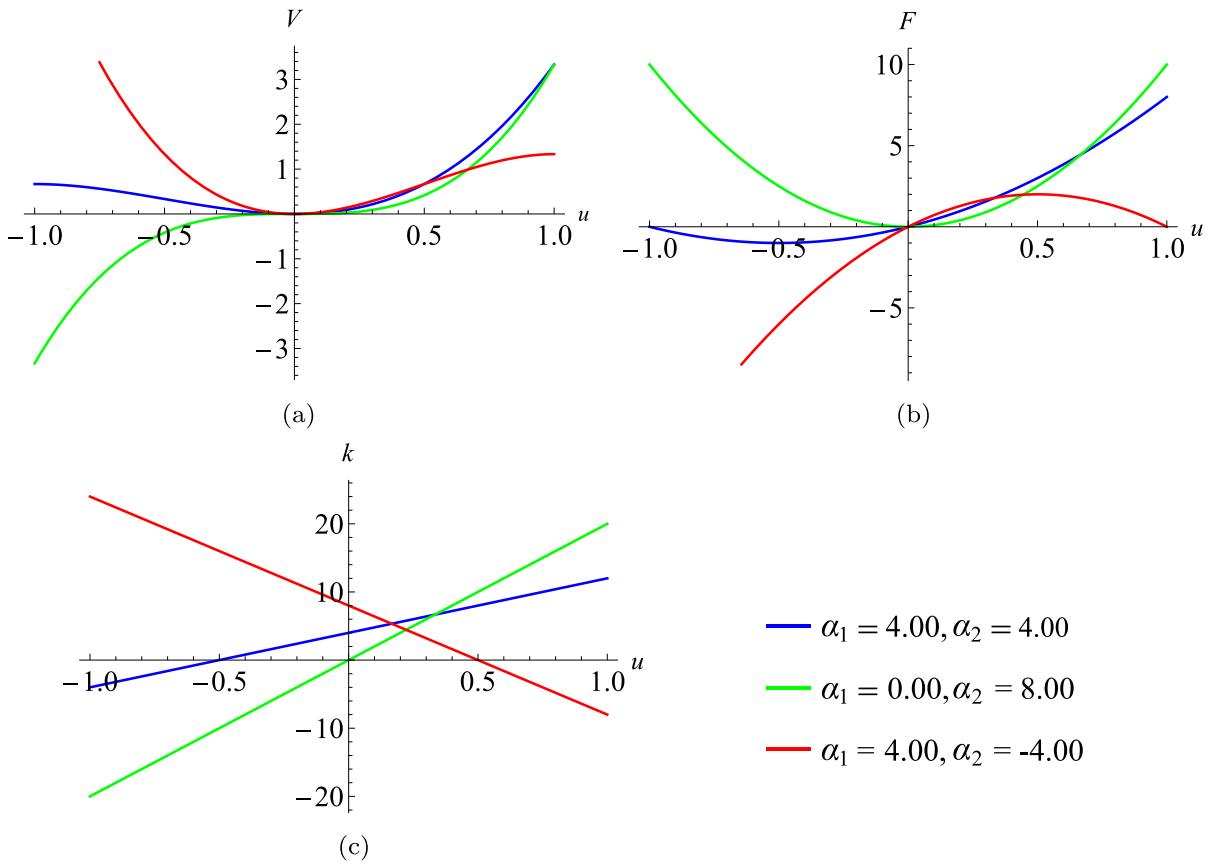

Fig. 3 V versus u (**a**), F versus u (**b**) and k versus u (**c**) laws for selected values of the constitutive parameters α_1 and α_2

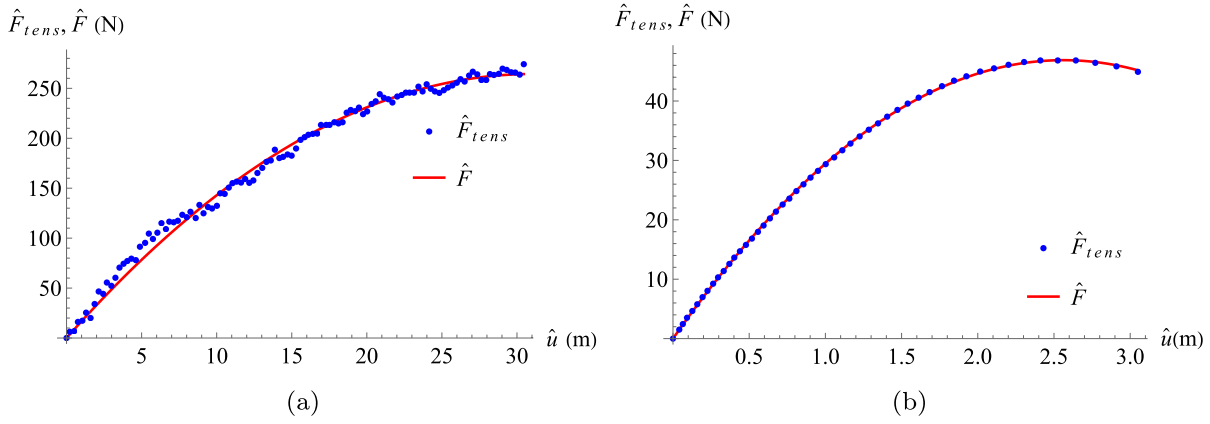

Fig. 4 Fitting of the tensegrity-like model (red curves) to the experimental response given in [20] for unit #1 (blue points) (**a**) and numerical prediction of the response of unit #2 given in [6] (blue points) (**b**). The remarkable fitting in (**b**) is due to the fact that the numerical data are obtained via an incremental algorithm (Color figure online)

where V is the interaction potential, and m is the mass of the single unit. The equation of motion of the i-th unit reads

$$m\frac{d^2u_i}{dt^2} = V_u\big(u_{i+1}\big) - 2V_u\big(u_i\big) + V_u\big(u_{i-1}\big) \tag{6}$$

We now write u_i as the realization of a continuous function $u(x, t)$ in correspondence to the current time t and the initial position x_i the i-th mass (i.e., $u_i = u(x_i, t)$). Next, we use a discrete-to-continuum approach similar to that presented in [1, 25], which leads us to turn Eq. (6) into the following continuous equation

$$\frac{m}{h_{\epsilon_0}^2}u_{tt} = \mathcal{L}\{[V_u(u(x,t))]_{xx}\}, \tag{7}$$

where h_{ϵ_0} is the equilibrium distance, and the differential operator $\mathcal{L} \approx 1 + \frac{1}{12}h_{\epsilon_0}^2\partial_{xx}$ takes into account the discreteness of the system under examination.

Two possible approaches can be employed to further manipulate Eq. (7). One available possibility is to employ the standard quasi-continuum approach followed in [13, 14] for stiffening-type systems (weakly non-linear approach). By considering $\epsilon << 1$ and $u \sim \epsilon u$, such an approach requires a the Taylor expansion of the real $F(u)$ in Eq. (4) in order to neglect terms of order greater than $\mathcal{O}(\epsilon^3 h_{\epsilon_0}^2)$. In the present case, such an expansion is actually not needed, since we are employing a cubic interaction potential. Therefore we are led directly to obtain the classical Boussinesq equation

$$\frac{m}{h_{\epsilon_0}^2}u_{tt} = \alpha_1 u_{xx} + \alpha_2(u^2)_{xx} + \frac{1}{12}h_{\epsilon_0}^2\alpha_1 u_{xxxx}. \tag{8}$$

The second approach consists of using Rosenau's [1] idea to invert the operator $\mathcal{L}$, obtaining

$$\mathcal{L}^{-1} \approx \left(1 - \frac{1}{12}h_{\epsilon_0}^2\partial_{xx}\right)$$

Applying such an operator to the linear term u_{tt} leads us, after some standard manipulations, to the following improved Boussinesq equation [1]

$$\frac{m}{h_{\epsilon_0}^2}u_{tt} = \alpha_1 u_{xx} + \alpha_2(u^2)_{xx} + \frac{1}{12}mu_{xxtt}. \tag{9}$$

It is worth noting that the speed for linear longitudinal waves (c_ℓ) is the same for Eqs. (8) and (9), being given by

$$c_\ell^2 = h_{\epsilon_0}^2\frac{\alpha_1}{m}$$

Nevertheless, the dispersion equation arising when we consider the fourth order derivative term is different for the two approaches under examination. Introducing the dimensionless unknown $\epsilon = u/h_{\epsilon_0}$ and the independent dimensionless variables $\tau = t/T$ and $\xi = x/h_{\epsilon_0}$ where T is a characteristic time and h_{ϵ_0} is a characteristic length, we rewrite the above differential equations as follows

$$\epsilon_{\tau\tau} = \epsilon_{\xi\xi} + \beta(\epsilon^2)_{\xi\xi} + \gamma\epsilon_{\xi\xi\xi\xi}, \tag{10}$$

and

$$\epsilon_{\tau\tau} = \epsilon_{\xi\xi} + \beta(\epsilon^2)_{\xi\xi} + \gamma\epsilon_{\xi\xi\tau\tau}. \tag{11}$$

Here, we have set

$$\frac{h_{\epsilon_0}^2}{T^2} = c_\ell^2$$

and

$$\beta = \frac{\alpha_2 h_{\epsilon_0}}{\alpha_1}, \quad \gamma = \frac{1}{12}$$

For these equations we are interested in finding a traveling *pulse* of the form $\epsilon = \phi(\xi - v\tau)$. Using such an ansatz, it is well known that the pulse solution for both (10) and (11) takes the form [22]

$$\epsilon(\xi,\tau) = A\,\mathrm{sech}^2\big[B(\xi - v\tau) + c_0\big], \tag{12}$$

where in both cases the amplitude A is given by

$$A = \frac{3}{2}\frac{v^2 - 1}{\beta}, \tag{13}$$

while the coefficient B is computed as follows for Eq. (10)

$$B^2 = \frac{v^2 - 1}{4\gamma} \tag{14}$$

and in the form

$$B^2 = \frac{v^2 - 1}{4\gamma v^2}. \tag{15}$$

for Eq. (11). Therefore, in both cases, the pulses supported by the tensegrity-like model under consideration are supersonic and 'dark' [26], since the assumption of softening-type response implies $\beta < 0$ (cf. Section 2). Restricting our analysis to cases in which the lattice remains under a nonzero level of compression, while rarefaction pulses propagate along the longitudinal axis, we must impose the constraint $|A| \leq |u_0/h_{\epsilon_0}|$. Using Eq. (13), such a condition implies that the traveling pulse must show a traveling speed not larger than the following limiting value

$$c_{max} = c_\ell \sqrt{\frac{2}{3}\frac{\beta\, u_0}{h_{\epsilon_0}} + 1} \tag{16}$$

Equation (12) allows us to give a simple and effective mathematical formulation to dark solitary waves in tensegrity lattice structures that exhibit softening-type response. It is worth noting that such waves have a shape similar to that exhibited by the depression solitary waves presented in [27] for the Korteweg-de Vries wave equation in the subsonic regime. Moreover, we observe that Eq. (12) provides an accurate approximation to the rarefaction solitary pulses obtained by Herbold and Nesterenko in [10]. Figure 5 shows a comparison between the pulse illustrated in Fig. 3 of such a reference, for a lattice endowed with a power-lave interaction potential featuring an exponent $n = 1/2$, and a sech^2 pulse with $-A = \epsilon_0 = 0.033$ and $B = 0.85$. The vertical axis gives the total strain $\hat{\epsilon} = \hat{u}/h_0 = \epsilon + \epsilon_0(1 - \epsilon)$. A rather good matching between the profiles of such pulses can be observed in Fig. 5.

5 Comparisons with previous numerical studies

We study in the present section the continuum limit of a chain of $T3$ units #2 that features a pre-compression strain $\epsilon_0 = 0.15$. It is useful to establish a comparison between the predictions of a tensegrity-like approach to the wave dynamics of such a system, and the numerical results presented in Table S2 of [6] for a mass-spring chain consisting of 1400 prisms equipped with the properties listed in Table 2. Figure 3 of Ref. [6] graphically illustrates the propagation of rarefaction pulses in the tensegrity chain under consideration, which are produced by the application of an initial compression disturbance at one end of the chain. Such rarefaction pulses are followed by oscillatory tails that progressively shrink in amplitude during the propagation of the leading pulses.

We now compare the shape and speed of the rarefaction pulses predicted by the tensegrity-like theory presented in the previous section, which make use of Eq. (12)–(15) and the constitutive parameters given in Sect. 3, with the numerical results presented in [6]. It is useful to compare 'theoretical' and 'numerical' rarefaction waves with equal peak amplitudes, with the aim of assessing the ability of

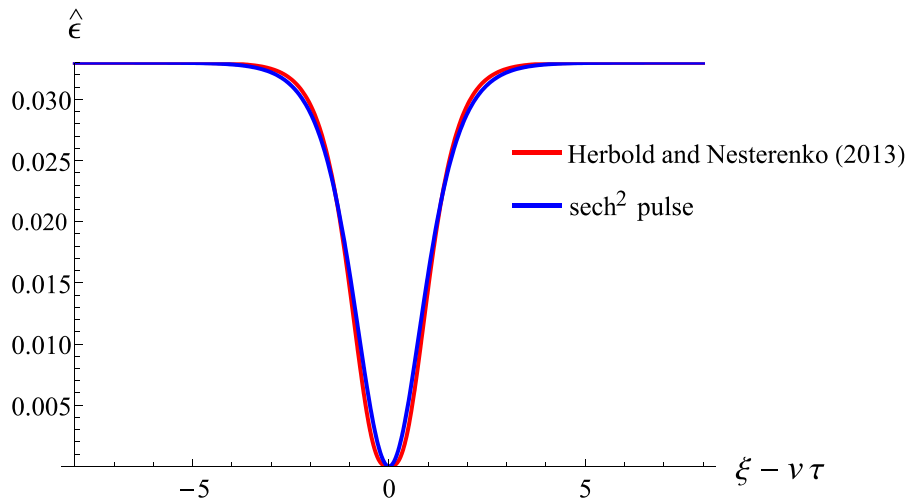

Fig. 5 Comparison between the sech^2 pulses predicted by the tensegrity-like approach and the profiles of the solitary pulses analyzed in [10], for $\epsilon_0 = 0.033$

the tensegrity-like approach in predicting the wave speed and the wave width of the rarefaction pulses (see Table 3). The wave widths corresponding to the Boussinesq Equation (BE: Eq. (10)) and the Improved Boussinesq Equation (IBE: Eq. (11)) were computed assuming a cutoff of $\hat{\epsilon}$ equal to 0.02 ϵ_0. The results illustrated in Table 3 highlight a rather good matching between theoretical and numerical results. One notes, in particular, that the wave width reduces with increasing values of the wave speed, in both the analyzed models. It is also observed that the IBE model predicts slightly larger wave widths as compared to the BE model. The waveform of the tensegrity-like pulses is shown in Fig. 6 for different wave speeds $c = v\, c_\ell$, which range from a value close to the sound speed for linear longitudinal waves (1.02 c_ℓ), up to c_{max} (1.13 c_ℓ).

6 Concluding remarks

This work has investigated the existence and the properties of rarefaction pulses propagating through tensegrity-like mass-spring chains subject to an initial pre-compression, which are equipped with a cubic FPU interaction potential. The latter proved to accurately capture the constitutive response of $T3$ tensegrity prisms featuring a softening-type response under compression loading [6, 20]. Two analytical models have been proposed to predict the propagation of rarefaction solitary pulses in the examined tensegrity-like mass-spring chains, making use of the classical Boussinesq wave equation, and an improved version of such an equation proposed by Rosenau [1]. Analytic formulae have been provided for the shape and the propagation speed of the above pulses, which produce a reduction of the initial state of pre-compression of the system. Interestingly, the presented results

Table 3 Comparison between theoretical and numerical results for the propagation of rarefaction pulses in a tensegrity mass-spring chain with softening response

Peak amplitude $A + \epsilon_0\,(1 - A)$		Wave speed	Wave width
0.122	Boussinesq equation	1.02 c_ℓ	9.18
	Improved Boussinesq equation		9.41
	Reference [6]	1.00 c_ℓ	12.00
0.040	Boussinesq equation	1.09 c_ℓ	6.46
	Improved Boussinesq equation		7.07
	Reference [6]	1.08 c_ℓ	10.00
0	Boussinesq equation	1.13 c_ℓ	5.89
	Improved Boussinesq equation		6.63

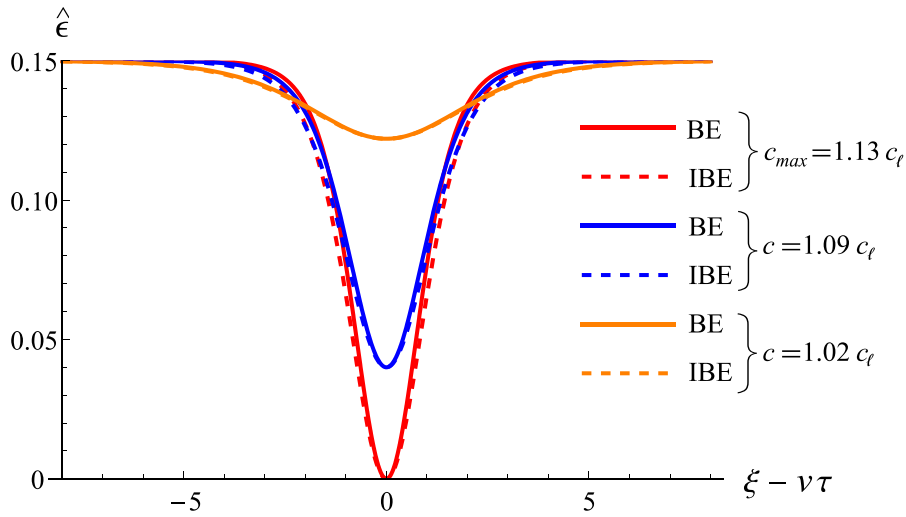

Fig. 6 Profiles of the solitary pulses traveling with different speeds through a chain formed by lumped masses and the $T3$ units #2, for $\epsilon_0 = 0.15$

closely approximate those obtained for the dark solitary pulses studied in [10], and the numerical results presented in [6] for a micro-scale tensegrity mass-spring chain with softening response.

We address studies dealing with the stability properties of rarefaction solitary waves propagating in tensegrity lattices to future work [28, 29]. Additional lines of future research will include the study of mechanical metamaterial applications of the studied behaviors, with the aim of developing innovative bandgap systems [5, 17], and ground-breaking impact protection devices that are able to transform impulsive compression loading into rarefaction waves. A tensegrity structure will be used to redirect energy from an incident shock into a compact-support rarefaction wave, characterized by a gradually diminishing oscillatory tail. This effect will be achieved through a softening-type geometric nonlinearity, which will be adjusted using local and global prestress [6]. Future studies will involve the mechanical modeling of a composite system, consisting of a tensegrity lattice embedded in a matrix material, which acts as a porous medium [30]. Additionally, we plan to investigate the incorporation of inertial effects into tensegrity-like systems, aiming to achieve bandgap effects at low frequencies [31].

Acknowledgements The authors acknowledge support by the Italian National Group of Mathematical Physics (GNFM), and the 'Istituto Nazionale di Alta Matematica Francesco Severi' (INdAM).

Funding Open access funding provided by Università degli Studi di Perugia within the CRUI-CARE Agreement. This research has been funded under the National Recovery and Resilience Plan (NRRP), by the European Union - NextGenerationEU, within the project with grant number P2022CR8AJ (FF PI). This research has also been funded by the NextGenerationEU PRIN2022 research projects with grant numbers 2022P5R22A (GS PI) and 20224LBXMZ (FF PI). FF also acknowledges the support by the Italian Ministry of Foreign Affairs and International Cooperation within the Italy-USA Science and Technology Cooperation Program 2023–2025, Project "Next-generation green structures for natural disaster-proof buildings" (grant n. US23GR15).

References

1. Rosenau P (1986) Dynamics of nonlinear mass-spring chains near the continuum limit. Phys Lett A 118(5):222–227
2. Nesterenko VF (2013) Dynamics of heterogeneous materials. Springer
3. Destrade M, Gaeta G, Saccomandi G (2007) Weierstrass's criterion and compact solitary waves. Phys Rev E 75:047601
4. Rubin M, Rosenau P, Gottlieb O (1995) Continuum model of dispersion caused by an inherent material characteristic length. J Appl Phys 77(8):4054–4063
5. Amendola A, de Castro Motta J, Saccomandi G, Vergori L (2024) A constitutive model for transversely isotropic dispersive materials. Proc R Soc A 480(2281):20230374
6. Fraternali F, Carpentieri G, Amendola A, Skelton RE, Nesterenko VF (2014) Multiscale tunability of solitary wave dynamics in tensegrity metamaterials. Appl Phys Lett 105(20):201903
7. Liu Y, Bartal G, Genov DA, Zhang X (2007) Subwavelength discrete solitons in nonlinear metamaterials. Phys Rev Lett 99(15):153901
8. Nesterenko VF (1984) Propagation of nonlinear compression pulses in granular media. J Appl Mech Tech Phys (Engl Transl) 24(5):733–743
9. Porter MA, Daraio C, Szelengowicz I, Herbold EB, Kevrekidis P (2009) Highly nonlinear solitary waves in heterogeneous periodic granular media. Physica D 238(6):666–676
10. Herbold EB, Nesterenko VF (2013) Propagation of rarefaction pulses in discrete materials with strain-softening behavior. Phys Rev Lett 110(14):144101
11. Daraio C, Fraternali F (2013) Method and apparatus for wave generation and detection using tensegrity structures, US Patent 8,616,328
12. Micheletti A, Ruscica G, Fraternali F (2019) On the compact wave dynamics of tensegrity beams in multiple dimensions. Nonlinear Dyn 98(4):2737–2753
13. Amendola A (2023) An analytic study on the properties of solitary waves traveling on tensegrity-like lattices. Int J Non-Linear Mech 148:104264
14. de Castro Motta J, Garanger K, Rimoli JJ (2024) Propagation of compression solitary waves on tensegrity-like lattices made of truncated octahedrons. Int J Non-Linear Mech 162:104716
15. Pal RK, Ruzzene M, Rimoli JJ (2018) Tunable wave propagation by varying prestrain in tensegrity-based periodic media. Extreme Mech Lett 22:149–156
16. Liu K, Zegard T, Pratapa PP, Paulino GH (2019) Unraveling tensegrity tessellations for metamaterials

with tunable stiffness and bandgaps. J Mech Phys Solids 131:147–166
17. Placidi L, de Castro Motta J, Fraternali F (2024) Bandgap structure of tensegrity mass-spring chains equipped with internal resonators. Mech Res Commun. (**In press**)
18. Miniaci M, Mazzotti M, Amendola A, Fraternali F (2021) Effect of prestress on phononic band gaps induced by inertial amplification. Int J Solids Struct 216:156–166
19. Skelton RE, De Oliveira MC (2009) Tensegrity systems, vol 1. Springer, Berlin
20. Amendola A, Carpentieri G, De Oliveira M, Skelton R, Fraternali F (2014) Experimental investigation of the softening-stiffening response of tensegrity prisms under compressive loading. Compos Struct 117:234–243
21. Fermi E, Pasta P, Ulam S, Tsingou M (1955) Studies of the nonlinear problems, Tech. Rep., Los Alamos National Lab. (LANL), Los Alamos
22. Clarkson PA, Kruskal MD (1989) New similarity reductions of the Boussinesq equation. J Math Phys 30(10):2201–2213
23. Friesecke G, Wattis JA (1994) Existence theorem for solitary waves on lattices. Commun Math Phys 161(2):391–418
24. Friesecke G, Pego RL (1999) Solitary waves on FPU lattices: I. qualitative properties, renormalization and continuum limit. Nonlinearity 12(6):1601
25. Olver PJ, Stern A (2021) Dispersive fractalisation in linear and nonlinear Fermi-Pasta-Ulam-Tsingou lattices. Eur J Appl Math 32(5):820–845
26. Kivshar YS, Luther-Davies B (1998) Dark optical solitons: physics and applications. Phys Rep 298(2–3):81–197
27. Falcon E, Laroche C, Fauve S (2002) Observation of depression solitary surface waves on a thin fluid layer. Phys Rev Lett 89(20):204501
28. Berryman JG (1976) Stability of solitary waves in shallow water. Phys Fluids 19(6):771–777
29. Pego RL, Weinstein MI (1997) Convective linear stability of solitary waves for Boussinesq equations. Stud Appl Math 99(4):311–375
30. de Castro Motta J, Zampoli V, Chiriţă S, Ciarletta M (2024) On the structural stability for a model of mixture of porous solids. Math Methods Appl Sci 47(6):4513–4529
31. Bergamini A, Miniaci M, Delpero T, Tallarico D, Van Damme B, Hannema G, Leibacher I, Zemp A (2019) Tacticity in chiral phononic crystals. Nat Commun 10(1):4525